Electronic Supplementary Material (ESI) for Dalton Transactions.

Supporting information

Dinuclear ytterbium(III) benzamidinate complexes with bridging S_3^{2-}, Se_2^{2-} and Te_2^{2-} ligands: synthesis, structure and magnetic properties

Ying-Zhao Ma,* Lian Yu, Qi Zhou and Wensheng Fu,*

Chongqing Key Laboratory of Green Synthesis and Applications, College of Chemistry, Chongqing Normal University, Chongqing 401331, China.

Table of Contents

Crystallographic Appendix

Single-crystal X-ray diffraction studies for complex **1**, **2** and reducing agent [$L_2Yb(THF)_2$] were carried out with the use of a Bruker D8 VENTURE diffractometer with Mo-Kα radiation (λ = 0.71073 Å) at 100 K, and data for complex **3** were collected on Rigaku Supernova diffractometer with Mo-Kα radiation (λ = 0.71073 A) at 180 K. 100K data collection was tried for complex **3**, however, the crystals kept cracking until the measuring temperature was increased to 180 K. All structures were solved by using the program SHELXS/T[1] using Olex2.[2] The remaining non-hydrogen atoms were located from successive difference Fourier map calculations. The refinements were carried out by using full-matrix least-squares techniques on F2 by using the program SHELXL.[1] All hydrogen atom positions were generatedgeometrically and refined with isotropic temperature factors. Cambridge Crystallographic Data Centre contains the crystal structure with the following CCDC number 2337379 (**1**), 2337380 (**2**), 2337378 (**3**)

Molecular structure of [$L_2Yb(THF)_2$]

For a better comparisons of Yb-N bond lengths between complex **1**, **2** and **3**, and divalent Yb complex SET agent, [$L_2Yb(THF)_2$] was crystalized from toluene and the resulted bond lengths and angels are of minor difference to the reported analogue (Fig S1).

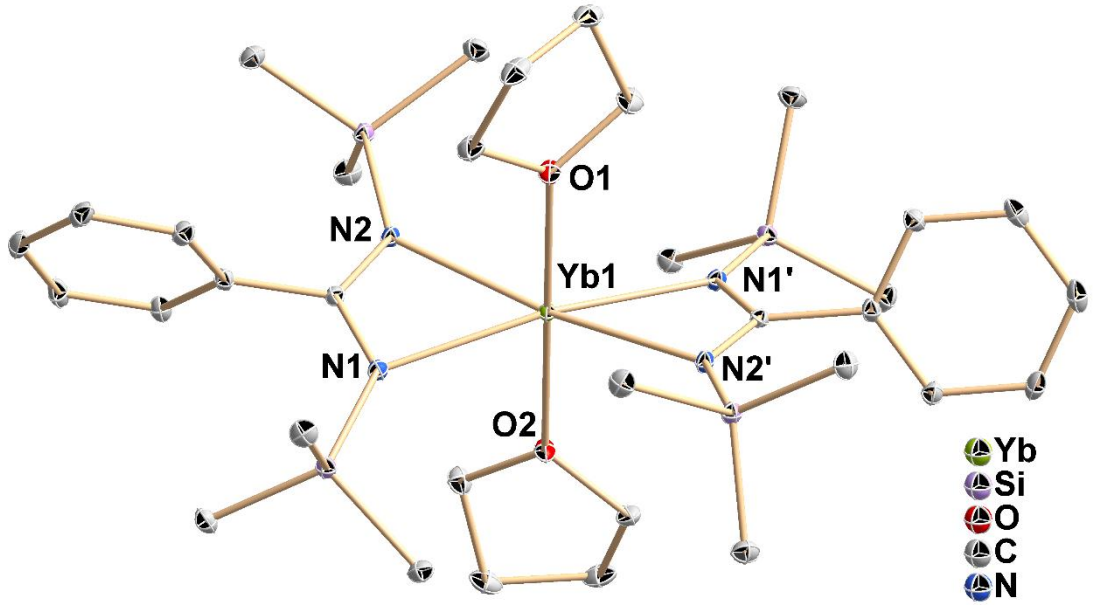

Fig. S1. Molecular structure of reproduced [$L_2Yb(THF)_2$] with 20% probability thermal ellipsoids. Hydrogen atoms and the disordered components have been omitted for clarity. Selected bond lengths (Å) Yb1-N1 2.476(2), Yb1-N1' 2.476(2), Yb1-N2 2.468(2), Yb1-N2' 2.468(2), Yb1-O1 2.421(3), Yb1-O2 2.398(3). Selected bond angles (º): O2-Yb1-O1 180.

Table S1. Crystallographic data and structural refinement parameters:

Complex	**$[L_2Yb(THF)_2]$**	**1**	**2**	**3**
Empirical formula	$C_{34}H_{62}N_4O_2Si_4Yb$	$C_{56}H_{100}N_8OS_3Si_8Yb_2$	$C_{60}H_{108}N_8O_2Se_2Si_8Yb_2$	$C_{66}H_{108}N_8Si_8Te_2Yb_2$
Formula weight	844.27	1568.41	1702.26	1839.60
CCDC number	1282646	2337379	2337380	2337380
Temperature/K	100	100	100	180
Crystal system	Orthorhombic	Monoclinic	Triclinic	Triclinic
Space group	*P*bcn	$P2_1/c$	$P\bar{1}$	$P\bar{1}$
a/Å	18.1831(7)	16.9080(7)	10.9290(10)	12.0836(2)
b/Å	12.8900(5)	14.7978(6)	17.2190(17)	13.4866(3)
c/Å	17.7620(5)	30.2287(12)	21.1806(17)	15.6191(3)
α/°	90	90	73.462(4)	97.304(2)
β/°	90	101.055(2)	89.252(4)	109.927(2)
γ/°	90	90	89.738(4)	114.411(2)
Volume/ $Å^3$	4163.1(3)	7422.9(5)	3820.7(6)	2069.55(8)
Z	4	4	2	1
$\rho_{calc}g/cm^3$	1.347	1.403	1.480	1.476
μ/mm^{-1}	2.394	2.758	3.553	3.092
F(000)	1744	3200	1720	916
Crystal size/mm^3	0.03 × 0.02 × 0.01	0.03 × 0.02 × 0.01	0.03× 0.02 × 0.02	0.03 × 0.02 × 0.01
radiation (λ, Å)	Mo Kα (0.71073)	Mo Kα (0.71073)	Mo Kα (0.71073)	Mo Kα (0.71073)
Θ_{min}/°	2.251	2.436	2.234	3.286
Θ_{max}/°	30.519	30.653	25.509	29.351
Reflections collected	30609	78334	48630	45086
Independent reflections	6256	22696	13749	10216
Reflections Used	9873	9802	9783	23384
R_{int}	0.0439	0.0684	0.0528	0.0425
Parameters	212	1166	802	401
Restraints	0	1914	86	0
Largest Peak	1.217	2.355	2.294	0.723
Deepest Hole	-1.055	-2.960	-2.092	-0.718
GOOF	1.131	1.123	1.092	1.055
wR_2 (all data)	0.0870	0.1924	0.1667	0.0559
wR_2	0.0661	0.1794	0.1571	0.0529
R_1 (all data)	0.0481	0.1228	0.0742	0.0318
R_1	0.0272	0.0918	0.0635	0.0269

Table S2. Selected bond lengths [Å] and angles [°] for **1**

Yb(1)-S(1)	2.698(2)	Yb(1)-N(3)	2.313(9)	Yb(2)-N(6)	2.290(7)
Yb(1)-S(2)	2.808(3)	Yb(1)-N(4)	2.319(7)	Yb(2)-N(7)	2.320(11)
Yb(1)-S(3)	2.863(2)	Yb(2)-S(1)	5.178(3)	Yb(2)-N(7A)	2.335(15)
Yb(1)-N(1)	2.241(13)	Yb(2)-S(2)	3.702(3)	Yb(2)-N(8)	2.337(8)
Yb(1)-N(1A)	2.530(19)	Yb(2)-S(3)	2.749(2)	S(1)-S(2)	2.072(4)
Yb(1)-N(2)	2.349(13)	Yb(2)-O(1)	2.318(5)	S(2)-S(3)	2.095(4)
Yb(1)-N(2A)	2.34(2)	Yb(2)-N(5)	2.315(8)		

S(1)-Yb(1)-S(2)	44.15(8)	N(4)-Yb(1)-N(2)	91.8(3)
S(1)-Yb(1)-S(3)	73.31(7)	N(4)-Yb(1)-N(2A)	97.3(6)
S(2)-Yb(1)-S(3)	43.34(8)	O(1)-Yb(2)-S(3)	92.71(15)
N(1)-Yb(1)-S(1)	106.5(4)	O(1)-Yb(2)-N(7)	88.1(9)
N(1)-Yb(1)-S(2)	91.3(4)	O(1)-Yb(2)-N(7A)	86.4(16)
N(1)-Yb(1)-S(3)	116.1(4)	O(1)-Yb(2)-N(8)	91.7(2)
N(1)-Yb(1)-N(2)	58.8(5)	N(5)-Yb(2)-S(3)	102.7(2)
N(1)-Yb(1)-N(3)	147.1(4)	N(5)-Yb(2)-O(1)	100.9(2)
N(1)-Yb(1)-N(4)	98.9(4)	N(5)-Yb(2)-N(7)	99.3(5)
N(1A)-Yb(1)-S(1)	108.1(4)	N(5)-Yb(2)-N(7A)	108.4(9)
N(1A)-Yb(1)-S(2)	80.3(4)	N(5)-Yb(2)-N(8)	157.5(3)
N(1A)-Yb(1)-S(3)	97.2(4)	N(6)-Yb(2)-S(3)	96.6(2)
N(2)-Yb(1)-S(1)	96.5(3)	N(6)-Yb(2)-O(1)	160.0(3)
N(2)-Yb(1)-S(2)	124.0(3)	N(6)-Yb(2)-N(5)	59.8(3)
N(2)-Yb(1)-S(3)	167.3(3)	N(6)-Yb(2)-N(7)	90.0(9)
N(2A)-Yb(1)-S(1)	99.9(6)	N(6)-Yb(2)-N(7A)	94.7(15)
N(2A)-Yb(1)-S(2)	111.5(6)	N(6)-Yb(2)-N(8)	105.0(3)
N(2A)-Yb(1)-S(3)	149.5(5)	N(7)-Yb(2)-S(3)	157.4(5)
N(2A)-Yb(1)-N(1A)	55.8(6)	N(7)-Yb(2)-N(8)	62.4(5)
N(3)-Yb(1)-S(1)	96.11(19)	N(7A)-Yb(2)-S(3)	148.4(8)
N(3)-Yb(1)-S(2)	121.4(2)	N(7A)-Yb(2)-N(8)	53.5(9)
N(3)-Yb(1)-S(3)	93.0(2)	N(8)-Yb(2)-S(3)	95.1(2)
N(3)-Yb(1)-N(1A)	155.5(5)	S(2)-S(1)-Yb(1)	70.76(10)
N(3)-Yb(1)-N(2)	95.7(4)	S(1)-S(2)-Yb(1)	65.10(9)
N(3)-Yb(1)-N(2A)	117.5(6)	S(1)-S(2)-S(3)	105.77(13)
N(3)-Yb(1)-N(4)	58.5(3)	S(3)-S(2)-Yb(1)	69.73(9)
N(4)-Yb(1)-S(1)	154.0(2)	Yb(2)-S(3)-Yb(1)	165.65(10)
N(4)-Yb(1)-S(2)	142.3(2)	S(2)-S(3)-Yb(1)	66.92(10)
N(4)-Yb(1)-S(3)	100.7(2)	S(2)-S(3)-Yb(2)	98.77(11)
N(4)-Yb(1)-N(1A)	97.6(5)		

Table S3. Selected bond lengths [Å] and angles [°] for **2**

Yb(1)-Se(1)	2.8578(13)	Yb(1)-N(4)	2.403(10)	Yb(2)-N(5)	2.347(10)
Yb(1)-Se(1)#1	3.0082(13)	Se(1)-Se(1)#1	2.375(3)	Yb(2)-N(6)	2.390(10)
Yb(1)-O(1)	2.361(9)	Yb(2)-Se(2)	2.8578(13)	Yb(2)-N(7)	2.358(10)
Yb(1)-N(1)	2.348(10)	Yb(2)-Se(2)#2	2.9455(13)	Yb(2)-N(8)	2.300(10)
Yb(1)-N(2)	2.319(10)	Yb(2)-O(2)	2.362(9)	Se(2)-Se(2)#2	2.398(3)
Yb(1)-N(3)	2.371(10)				
Se(1)-Yb(1)-Se(1)#1	47.69(5)	Se(2)-Yb(2)-Se(2)#2	48.79(5)		
O(1)-Yb(1)-Se(1)#1	87.7(2)	O(2)-Yb(2)-Se(2)#2	126.4(2)		
O(1)-Yb(1)-Se(1)	92.4(2)	O(2)-Yb(2)-Se(2)	83.6(2)		
O(1)-Yb(1)-N(3)	83.6(3)	O(2)-Yb(2)-N(6)	80.9(3)		
O(1)-Yb(1)-N(4)	86.5(3)	N(5)-Yb(2)-Se(2)	108.6(2)		
N(1)-Yb(1)-Se(1)#1	79.3(2)	N(5)-Yb(2)-Se(2)#2	88.3(3)		
N(1)-Yb(1)-Se(1)	124.7(2)	N(5)-Yb(2)-O(2)	85.1(4)		
N(1)-Yb(1)-O(1)	100.9(3)	N(5)-Yb(2)-N(6)	57.4(3)		
N(1)-Yb(1)-N(3)	147.2(3)	N(5)-Yb(2)-N(7)	155.3(4)		
N(1)-Yb(1)-N(4)	90.0(3)	N(6)-Yb(2)-Se(2)#2	136.1(3)		
N(2)-Yb(1)-Se(1)#1	91.7(2)	N(6)-Yb(2)-Se(2)	159.9(3)		
N(2)-Yb(1)-Se(1)	102.5(3)	N(7)-Yb(2)-Se(2)#2	114.2(3)		
N(2)-Yb(1)-O(1)	159.2(4)	N(7)-Yb(2)-Se(2)	94.6(3)		
N(2)-Yb(1)-N(1)	58.7(4)	N(7)-Yb(2)-O(2)	89.1(4)		
N(2)-Yb(1)-N(3)	111.2(4)	N(7)-Yb(2)-N(6)	97.9(4)		
N(2)-Yb(1)-N(4)	89.5(3)	N(8)-Yb(2)-Se(2)#2	84.2(3)		
N(3)-Yb(1)-Se(1)#1	133.5(2)	N(8)-Yb(2)-Se(2)	111.6(2)		
N(3)-Yb(1)-Se(1)	87.1(2)	N(8)-Yb(2)-O(2)	144.2(4)		
N(3)-Yb(1)-N(4)	57.7(3)	N(8)-Yb(2)-N(5)	117.3(4)		
N(4)-Yb(1)-Se(1)#1	166.6(3)	N(8)-Yb(2)-N(6)	88.4(3)		
N(4)-Yb(1)-Se(1)	144.7(2)	N(8)-Yb(2)-N(7)	58.6(4)		
Yb(1)-Se(1)-Yb(1)#1	132.31(5)	Yb(2)-Se(2)-Yb(2)#2	131.21(5)		
Se(1)#1-Se(1)-Yb(1)#1	62.84(5)	Se(2)#2-Se(2)-Yb(2)#2	63.70(5)		
Se(1)#1-Se(1)-Yb(1)	69.48(6)	Se(2)#2-Se(2)-Yb(2)	67.52(5)		

Symmetry transformations used to generate equivalent atoms:

#1 -x+1,-y+1,-z #2 -x+2,-y+2,-z+1

Table S4. Selected bond lengths [Å] and angles [°] for **3**

Yb(1)-Te(1)#1	3.0702(2)	Yb(1)-N(2)	2.304(2)	Yb(1)-N(4)	2.312(2)
Yb(1)-Te(1)	3.1202(2)	Yb(1)-N(3)	2.295(2)	Te(1)-Te(1)#1	2.7865(3)
Yb(1)-N(1)	2.282(2)				

Te(1)#1-Yb(1)-Te(1)	53.497(6)	N(3)-Yb(1)-Te(1)#1	103.56(5)
N(1)-Yb(1)-Te(1)#1	149.52(5)	N(3)-Yb(1)-Te(1)	156.07(5)
N(1)-Yb(1)-Te(1)	97.32(6)	N(3)-Yb(1)-N(2)	100.15(8)
N(1)-Yb(1)-N(2)	59.96(8)	N(3)-Yb(1)-N(4)	59.74(8)
N(1)-Yb(1)-N(3)	106.33(8)	N(4)-Yb(1)-Te(1)#1	97.46(5)
N(1)-Yb(1)-N(4)	102.56(8)	N(4)-Yb(1)-Te(1)	111.93(5)
N(2)-Yb(1)-Te(1)	94.77(5)	Yb(1)#1-Te(1)-Yb(1)	126.503(6)
N(2)-Yb(1)-Te(1)#1	108.95(5)	Te(1)#1-Te(1)-Yb(1)	62.333(7)
N(2)-Yb(1)-N(4)	150.43(8)	Te(1)#1-Te(1)-Yb(1)#1	64.170(7)

Symmetry transformations used to generate equivalent atoms:

#1 -x+1,-y+1,-z+1

Table S5. Selected bond lengths [Å] and angles [°] for [$L_2Yb(THF)_2$]

Yb(1)-O(2)	2.398(3)	Yb(1)-N(1)#1	2.476(2)	Yb(1)-N(2)	2.468(2)
Yb(1)-N(1)	2.476(2)	Yb(1)-N(2)#1	2.468(2)	Yb(1)-O(1)	2.421(3)

O(2)-Yb(1)-N(1)#1	84.73(5)	N(2)#1-Yb(1)-N(1)	125.41(7)
O(2)-Yb(1)-N(1)	84.73(5)	N(2)-Yb(1)-N(1)#1	125.41(7)
O(2)-Yb(1)-N(2)	95.08(6)	N(2)-Yb(1)-N(2)#1	169.84(11)
O(2)-Yb(1)-N(2)#1	95.08(6)	O(1)-Yb(1)-N(1)	95.27(5)
O(2)-Yb(1)-O(1)	180	O(1)-Yb(1)-N(1)#1	95.27(5)
N(1)#1-Yb(1)-N(1)	169.46(10)	O(1)-Yb(1)-N(2)#1	84.92(6)
N(2)#1-Yb(1)-N(1)#1	55.72(7)	O(1)-Yb(1)-N(2)	84.92(6)
N(2)-Yb(1)-N(1)	55.72(7)		

Symmetry transformations used to generate equivalent atoms:

#1 -x+1,y,-z+1/2

Experimental section

General Considerations. All the manipulations of air- and water-sensitive reactions were performed with rigorous exclusion of oxygen and moisture in flame-dried Schlenk-type glassware either on a dual manifold Schlenk line, interfaced to a high vacuum (10^{-3} torr) line or in an argon-filled Vigor glove box. Toluene, *n*-hexane, benzene, THF and diethyl ether were dried by using a Vigor solvent purification system (VSPS-5), degassed, and stored over potassium mirrors (for toluene, n-Hexane and benzene) or 4A molecular sieves (for THF and diethyl ether). Deuterated solvents were stored over Na/K alloy, degassed by three freeze-pump-thaw cycles. Elemental analyses were carried out with an Elementar vario Micro cube. ATR-IR spectra were recorded on a Bruker Alpha II spectrometer with a Platinum attenuated total reflection (ATR) module in the glovebox. The signals were classified into different categories (vs = very strong, s = strong, m = medium, w = weak). [$L_2Yb(THF)_2$] was prepared according to a reported procedure.[3]

Synthesis of 1.

Toluene (20 ml) was condensed onto the mixture of [$L_2Yb(THF)_2$] (210 mg, 0.3 mmol) and S_8 (10 mg, 0.039 mmol) at -78℃. The resulting mixture was slowly warmed up to ambient temperature, during which course the colour change from deep red to light orange was noted instantly, and stirred for 12h. The resulting orange suspension was filtered into a 2-section ampoule and flame sealed. Light yellows were obtained by slow evaporation of the solvent at ambient temperature. Yield: 90 mg (41 %). IR (ATR): $\tilde{\nu}$ (cm^{-1}) = 2949 (m), 2893 (w), 1387 (vs), 1245 (s), 1163 (w), 1073 (w), 1030 (w), 989 (s), 918 (w), 829 (vs), 781 (m), 757 (s), 725 (m), 701 (m), 683 (w), 601 (w), 486 (s), 439 (m). Elemental analysis calcd. for [($C_{52}H_{92}N_8S_3Si_8Yb_2$)($C_4H_8O$)] (1568.44): C 42.88, H 6.43, N 7.14%. Found: C 42.47, H 6.56, N 7.31%.

Synthesis of 2.

By adopting the similar procedure for the preparation of **1** but using Selenium in place of elemental sulfur, complex 2 was obtained. Toluene (20 ml) was condensed onto a mixture of [$L_2Yb(THF)_2$] (140 mg, 0.2 mmol) and Se (16 mg, 0.2 mmol) at -78℃. The resulting mixture was slowly warmed up to ambient temperature and stirred for 48h. The color changes from deep red to orange after 1 hour and the resulting suspension was filtered into a 2-section ampoule and flame sealed. Orange crystals were obtained by slow evaporation of the solvent at ambient temperature. Light orange crystals were obtained at ambient temperature. Yield: 92 mg (59 %). IR (ATR): $\tilde{\nu}$ (cm-1) = 2951 (m), 2893 (w), 1422 (w), 1393 (s), 1241 (s), 1164 (w), 1073 (w), 1029 (w), 1003 (w), 983 (s), 918 (w), 828 (vs), 784 (m), 756 (s), 724 (w), 699 (m), 680 (w), 602 (w), 478 (s), 438 (m). Elemental analysis calcd. for ($C_{60}H_{108}N_8O_2Si_8Se_2Yb_2$) (1702.38): C 42.33 H 6.40 N 6.58%. Found: C 41.99 H 6.72 N 6.67%.

Synthesis of 3.

Toluene (20 ml) was condensed at room temperature onto a mixture of [$L_2Yb(THF)_2$] (70 mg, 0.1 mmol) and Te (13 mg, 0.1 mmol). Stirred the resulting mixture at room temperature for 12 hours. Concentrated the filtrate and dark green needle shaped crystals were obtained at -35 ℃. Yield: 43 mg (52 %). IR (ATR): $\tilde{\upsilon}$ (cm-1) = 2951 (m), 2893 (w), 1424 (w), 1397 (s), 1242 (s), 1168 (w), 1072 (w), 1004 (m), 983 (s), 919 (w), 829 (vs), 786 (m), 757 (s), 721 (m), 699 (m), 681 (w), 603 (m), 478 (s), 439 (m). Elemental analysis calcd. (%) for ($C_{52}H_{92}N_8Si_8Te_2Yb_2$) (1655.35): C 37.73 H 5.60 N 6.77. Found: C 37.91 H 5.81 N 6.91.

IR spectra

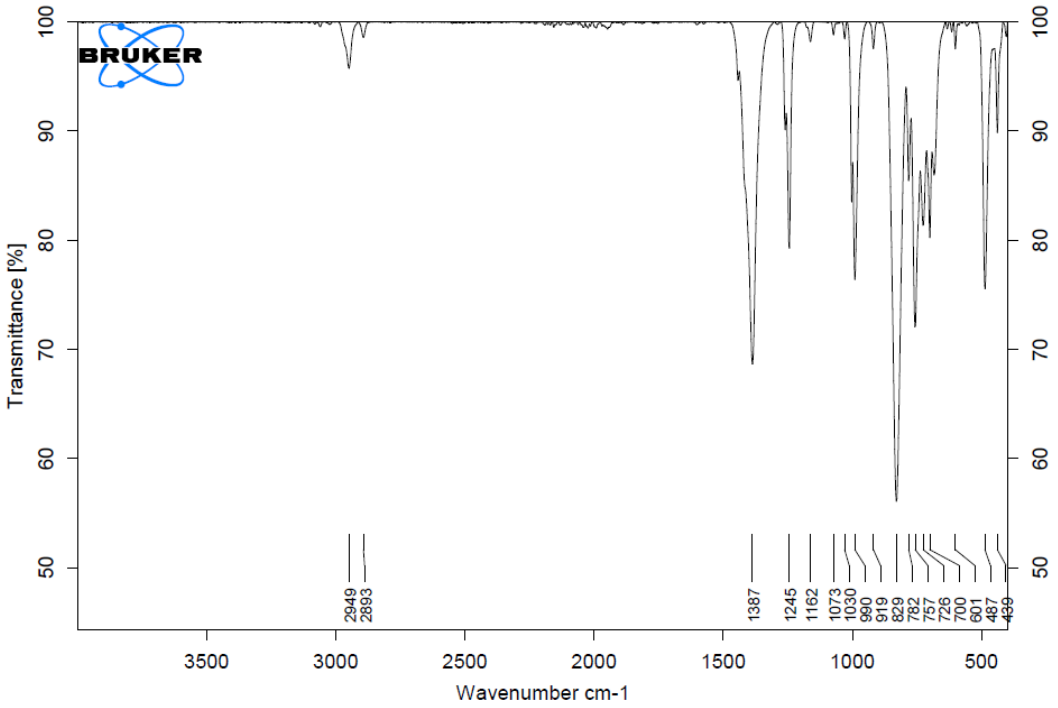

Fig. S2. IR spectra of **1**.

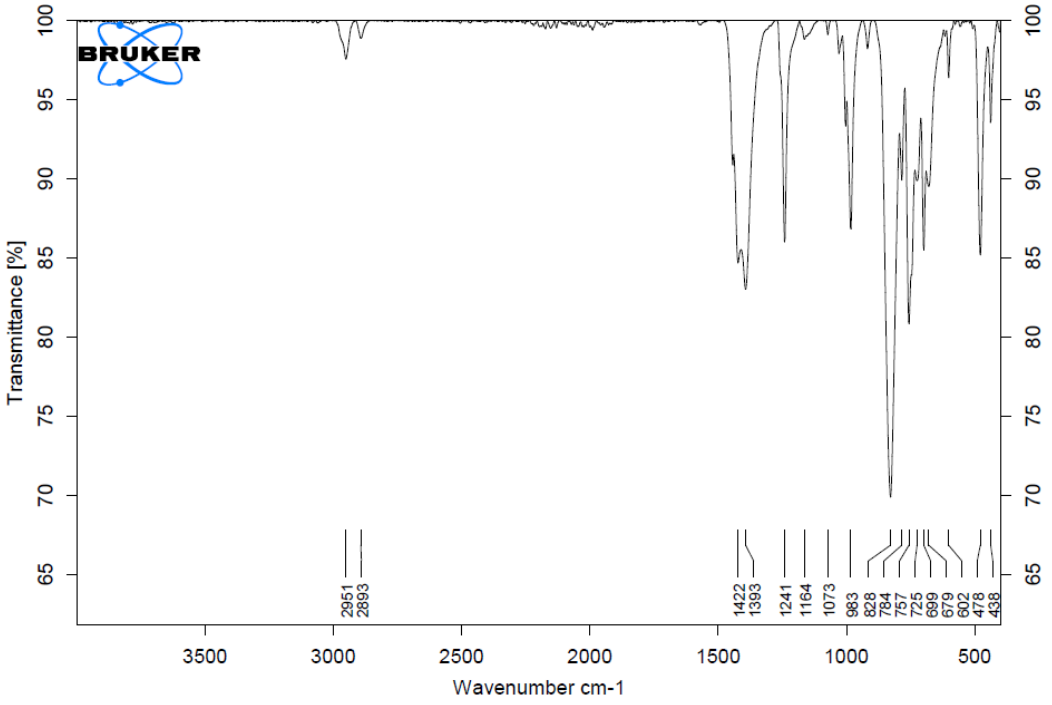

Fig. S3. IR spectra of **2.**

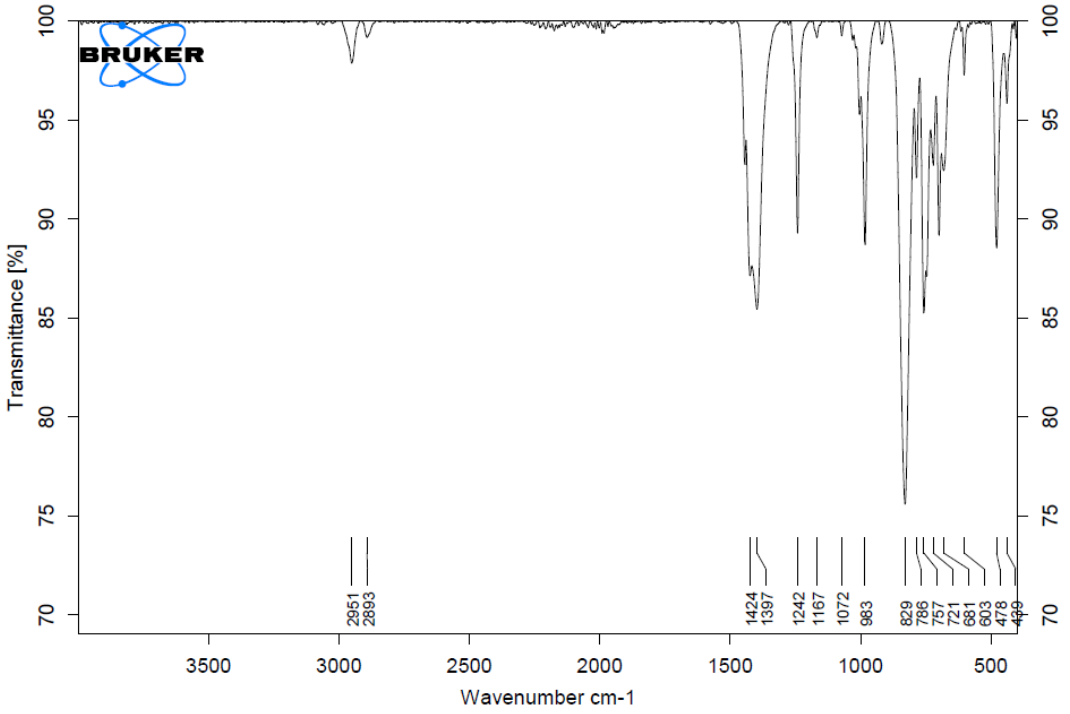

Fig. S4. IR spectra of **3.**

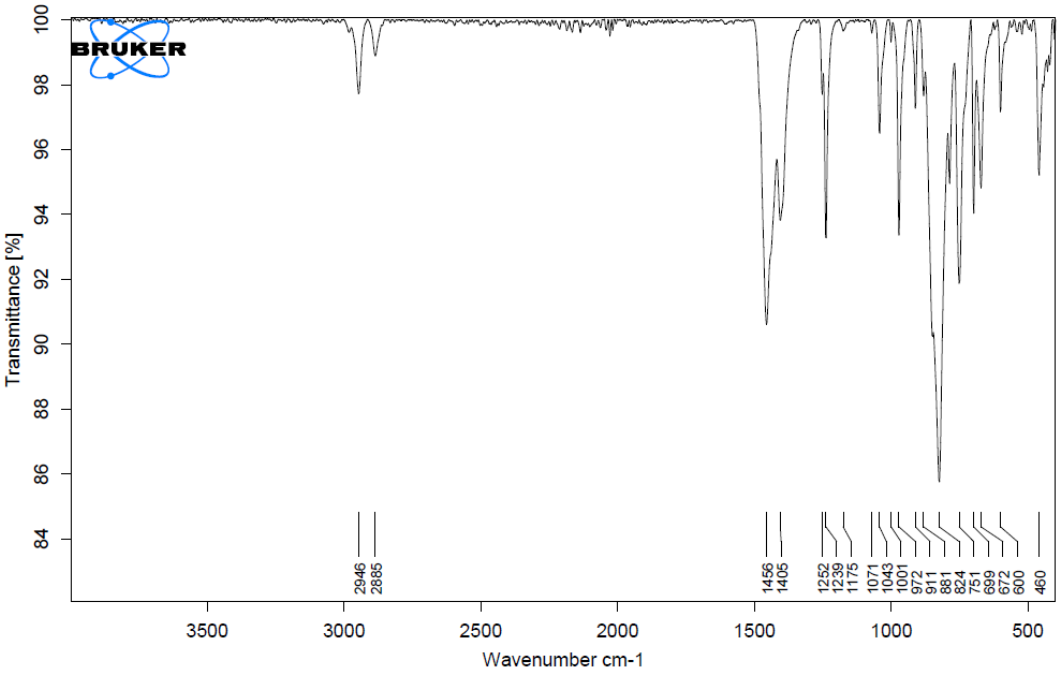

Fig. S5. IR spectra of **[$L_2Yb(THF)_2$]**.

Magnetic properties

Magnetic susceptibility measurements were carried out with a Quantum Design MPMS-3 SQUID magnetometer. Polycrystalline samples were sealed with melted eicosane in NMR tubes under vacuum. The standard AC magnetic susceptibility data were collected with a 3.5-Oe oscillating AC field.

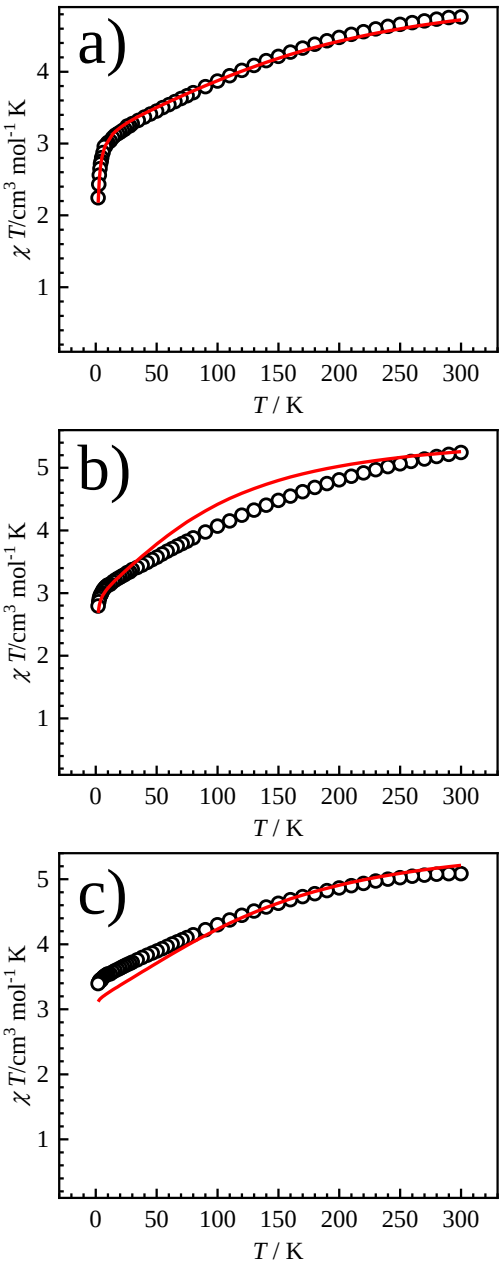

Fig. S6. The χT versus T plot of **1** (a), **2** (b) and **3** (c) under a DC field of 1000 Oe. Solid lines are best fits utilizing POLY_ANISO module (see computational section for details).

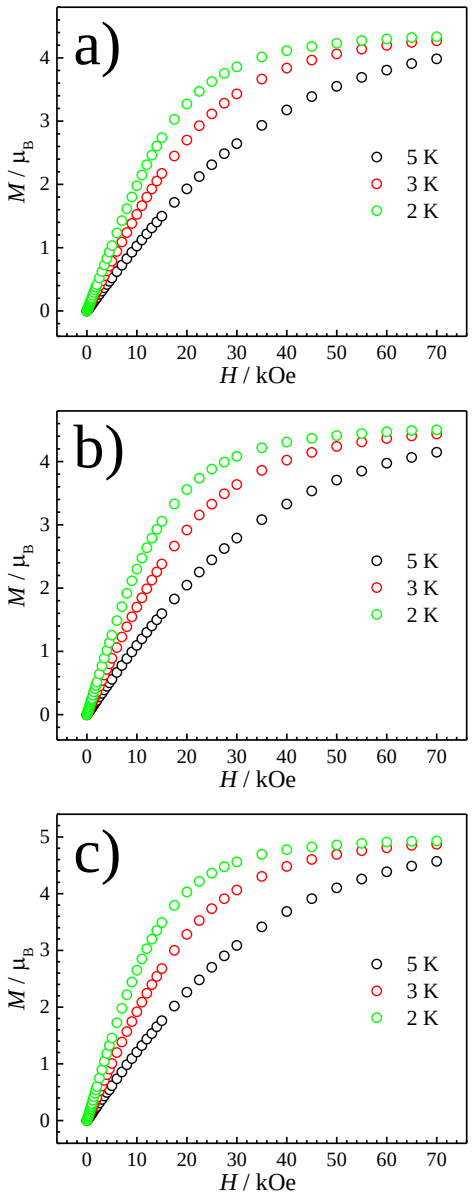

Fig. S7. The field-dependent magnetization plots at indicated temperatures for **1** (a), **2** (b) and **3** (c).

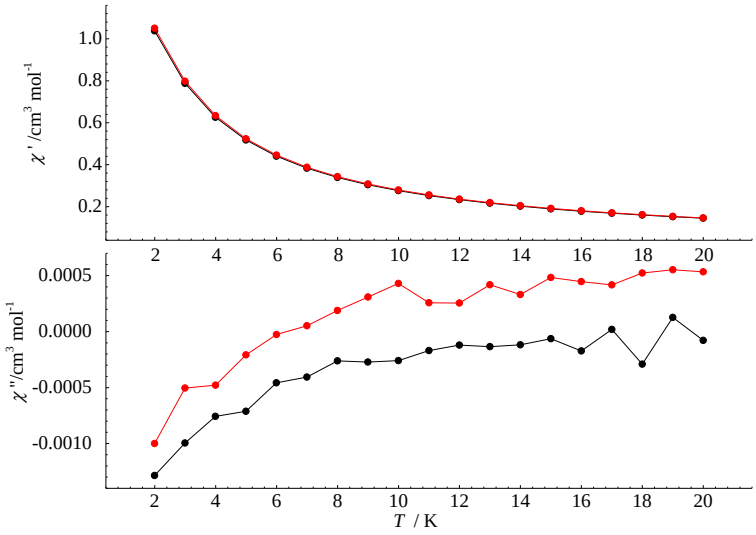

Fig. S8. Temperature-dependence of the in-phase (χ', top) and out-of-phase (χ'', bottom) AC susceptibility signals under zero DC field for **1** at frequencies of 77 Hz (black) and 777 Hz (red). Solid lines are guide for vision.

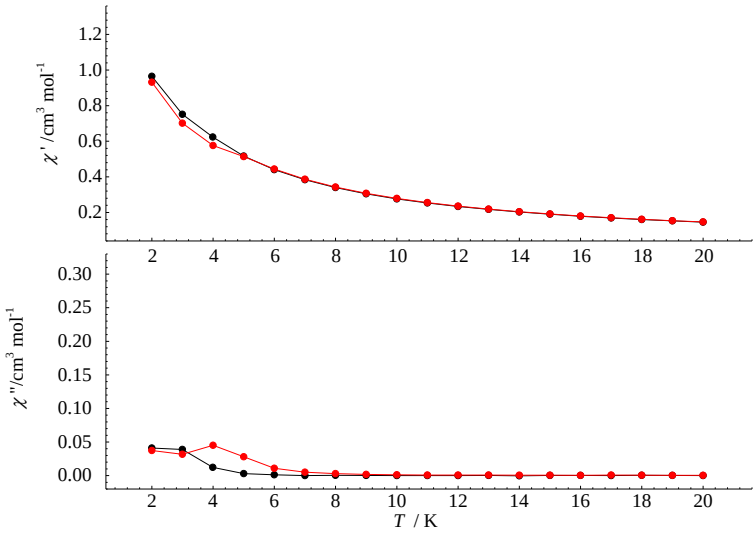

Fig. S9. Temperature-dependence of the in-phase (χ', top) and out-of-phase (χ'', bottom) AC susceptibility signals under 1000 Oe DC field for **1** at frequencies of 77 Hz (black) and 777 Hz (red). Solid lines are guide for vision.

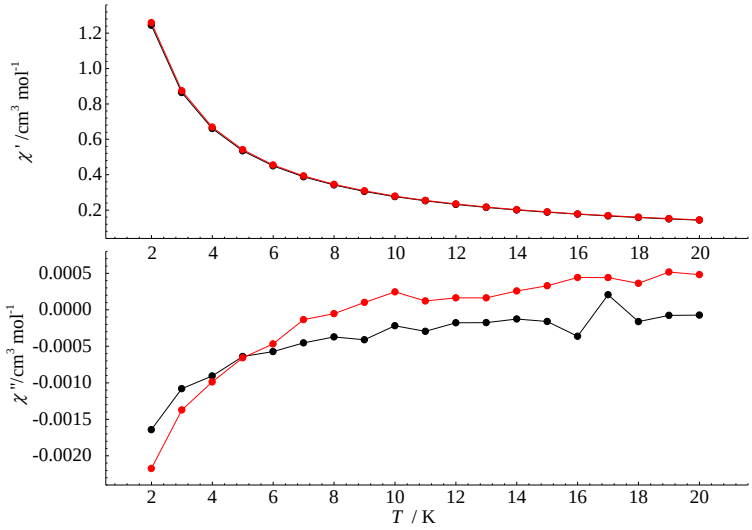

Fig. S10. Temperature-dependence of the in-phase (χ', top) and out-of-phase (χ", bottom) AC susceptibility signals under zero DC field for **2** at frequencies of 77 Hz (black) and 777 Hz (red). Solid lines are guide for vision.

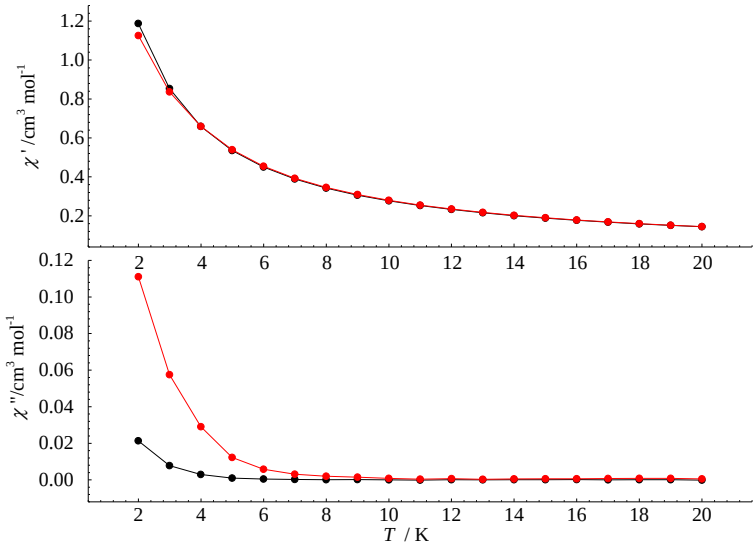

Fig. S11. Temperature-dependence of the in-phase (χ', top) and out-of-phase (χ", bottom) AC susceptibility signals under 1000 Oe DC field for **2** at frequencies of 77 Hz (black) and 777 Hz (red). Solid lines are guide for vision.

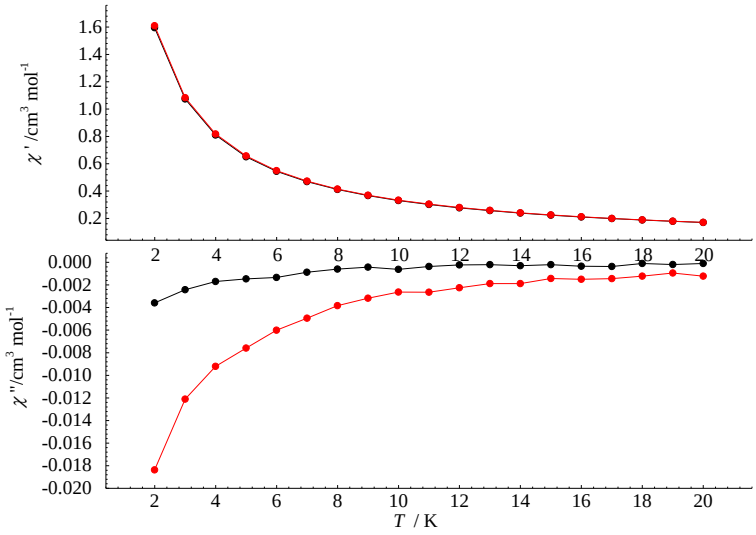

Fig. S12. Temperature-dependence of the in-phase (χ', top) and out-of-phase (χ", bottom) AC susceptibility signals under zero DC field for **3** at frequencies of 77 Hz (black) and 777 Hz (red). Solid lines are guide for vision.

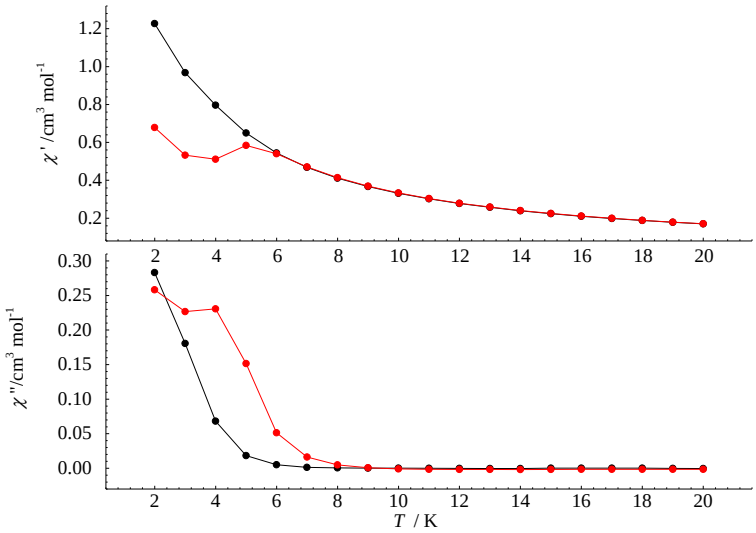

Fig. S13. Temperature-dependence of the in-phase (χ', top) and out-of-phase (χ", bottom) AC susceptibility signals under 1000 Oe DC field for **3** at frequencies of 77 Hz (black) and 777 Hz (red). Solid lines are guide for vision.

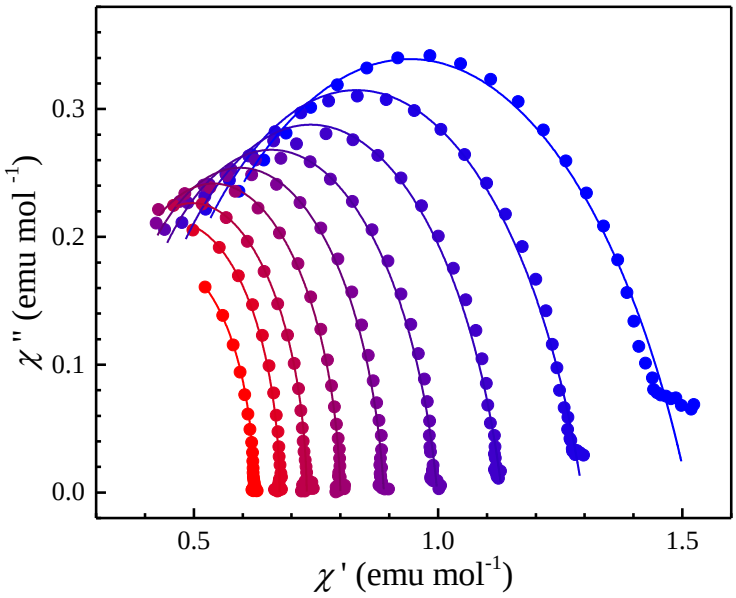

Fig. S14. Cole-Cole fit of **3** under an applied DC field of 1 kOe by standard AC susceptibility measurements.

Table S6. Relaxation fitting parameters obtained using a generalized Debye model for **3** from 2 K to 5.2 K under an applied DC field of 1 kOe.

T / K	*τ* / s	*τ*_err	*α*
2	7.23022E-4	2.85861E-5	0.3163
2.4	6.54882E-4	1.05756E-5	0.23873
2.8	5.7468E-4	9.44122E-6	0.19263
3.2	4.7222E-4	7.52469E-6	0.14903
3.6	3.67496E-4	5.37931E-6	0.09311
4	2.6736E-4	3.74743E-6	0.04554
4.4	1.86533E-4	4.38274E-6	0.02108
4.8	1.29566E-4	5.12086E-6	0
5.2	9.51797E-5	4.15968E-6	0

Computational Details

All the calculations were performed on *OpenMolcas* software package.[4] The coordinates of the major disordered components obtained from the single crystal structure (Figure S15-17) were used without optimization. The ab initio calculations were performed on trivalent Yb centre and the single ion anisotropy was calculated by replacing the paramagnetic lanthanide ion with diamagnetic Lu(III) ion. We employed the basis set from ANO-RCC library for all the calculations with VTZP quality for Yb atoms, VDZP quality for the N, S, Se and Te atoms, and VDZ quality for any remaining atoms. In addition, the Douglas-Kroll-Hess Hamiltonian has been used to include the relativistic effect.[5] To obtain the energy of the spin-free eigen states we have performed the complete active space self-consistence field (CASSCF) method by including 13 electrons in 7 4f orbitals for Yb(III) ion.[6] In this active space 7 doublets excited states have been considered in the configuration interaction procedure to compute the magnetic anisotropy of the single metal centres. Also, we used RASSI-SO7 to introduce the spin-orbit coupling within the space of the calculated spin-free eigen states for both compounds. Further to compute the g tensor and the crystal field parameters we have used the *Single_Aniso* module as implemented by considering previously calculated spin-orbit sates.[7] In addition, the Cholesky decomposition for 2-electron integrals was used throughout the calculations to save the disk space. The exchange interaction between the magnetic centres is considered within the Lines model, fitted through comparison of the computed and measured magnetic susceptibility using the POLY_ANISO program.[8]

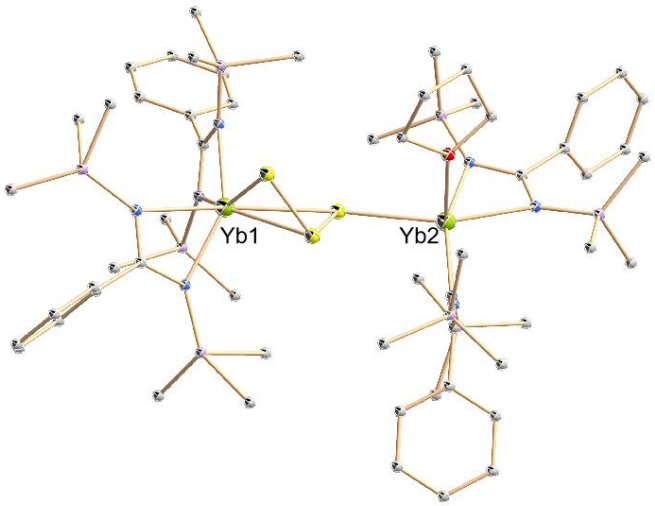

Fig. S15. Molecular structure of major disordered component in **1** shown with 20% probability thermal ellipsoids. Hydrogen atoms and the disordered components have been omitted for clarity.

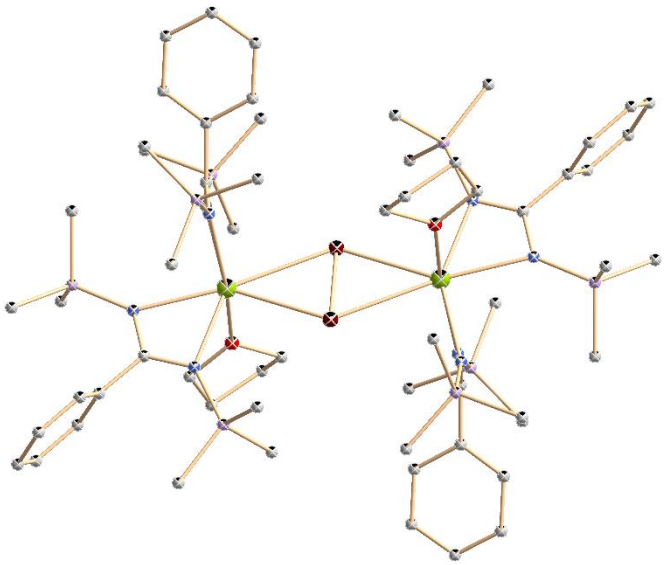

Fig. S16. Molecular structure of major disordered component in **2** shown with 20% probability thermal ellipsoids. Hydrogen atoms and the disordered components have been omitted for clarity.

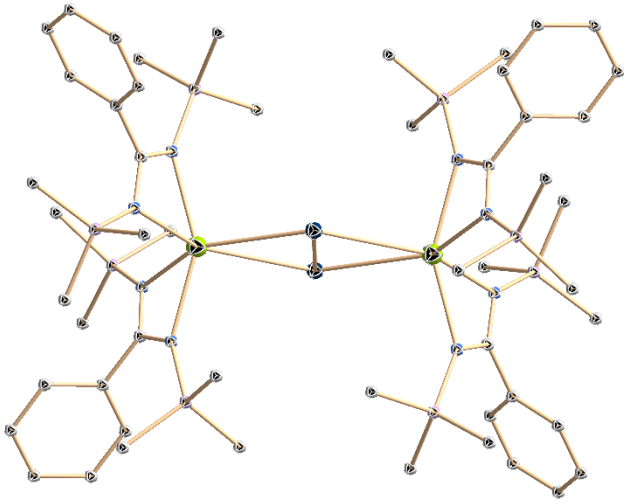

Fig. S17. Molecular structure of major disordered component in **3** shown with 20% probability thermal ellipsoids. Hydrogen atoms and the disordered components have been omitted for clarity.

Table S7. Single_Aniso computed crystal-field parameters for complex **1-3**.

k	Q	**1**		**2**	**3**
		Yb1	Yb2		
2	-2	-7.34E+00	1.70E+01	1.73E+00	-1.13E+00
2	-1	3.47E-01	6.37E-01	1.46E+01	-2.26E+01
2	0	-1.52E+01	-9.76E+00	1.30E+01	1.67E+01
2	1	-8.09E+00	-3.99E+00	2.61E+01	4.83E+00
2	2	8.20E+00	1.03E+01	-2.50E+00	-5.39E+00
4	-4	1.06E-01	3.00E-01	-5.02E-01	3.29E-01
4	-3	7.98E-01	8.70E-02	-1.02E+00	1.62E-01
4	-2	9.12E-03	8.03E-02	3.35E-02	-2.63E-02
4	-1	2.76E-01	7.72E-02	1.55E-01	-7.36E-01
4	0	-1.23E-01	-1.71E-01	-1.17E-01	-1.55E-01
4	1	3.87E-01	1.57E-01	5.61E-01	1.72E-01
4	2	2.61E-01	1.30E-01	-1.10E-02	-7.96E-02
4	3	2.52E-01	-4.32E-01	-1.03E+00	-3.21E-02
4	4	-9.43E-01	-1.13E+00	-2.98E-01	3.04E-01
6	-6	-2.84E-02	4.30E-02	7.67E-03	-4.23E-04
6	-5	-9.07E-03	9.00E-03	4.94E-02	2.32E-02
6	-4	5.79E-03	7.26E-03	3.66E-03	-4.92E-04
6	-3	1.92E-02	2.54E-03	-3.32E-02	3.07E-02
6	-2	1.37E-02	5.10E-03	-1.08E-02	5.14E-03
6	-1	3.91E-03	2.24E-03	-1.41E-02	-1.20E-02
6	0	-8.73E-04	-1.11E-05	3.76E-03	4.89E-03
6	1	-2.62E-02	1.48E-02	3.96E-03	2.01E-03
6	2	1.47E-02	-2.80E-03	-1.47E-02	1.14E-02
6	3	1.68E-02	-2.02E-02	5.15E-05	-2.14E-02
6	4	-2.28E-02	-2.58E-02	-6.82E-04	2.48E-03
6	5	-1.94E-02	8.31E-03	4.48E-03	-5.55E-02
6	6	5.05E-03	2.19E-02	-1.31E-03	-1.70E-03

Table S8. Single_Aniso computed energy of the KDs, g and wavefuctions composition for Yb1 in **1**.

Energy (cm^{-1})	g_x	g_y	g_z	**Wavefunction**
0.00	0.57	1.12	7.33	$91.9\%\|\pm 7/2\rangle + 3.8\%\|\pm 1/2\rangle + 3.1\%\|\pm 3/2\rangle + 1.2\%\|\pm 5/2\rangle$
394.746	1.16	2.29	4.62	$62.7\%\|\pm 5/2\rangle + 20.4\%\|\pm 3/2\rangle + 12.5\%\|\pm 1/2\rangle + 4.4\%\|\pm 7/2\rangle$
538.349	1.11	1.94	5.98	$38.5\%\|\pm 1/2\rangle + 37.2\%\|\pm 3/2\rangle + 21.9\%\|\pm 5/2\rangle + 2.4\%\|\pm 7/2\rangle$
708.566	7.95×10^{-2}	0.46	7.42	$45.2\%\|\pm 1/2\rangle + 39.2\%\|\pm 3/2\rangle + 14.2\%\|\pm 5/2\rangle + 1.3\%\|\pm 7/2\rangle$

Table S9. Single_Aniso computed energy of the KDs, g and wavefuctions composition for Yb2 in **1**.

Energy (cm^{-1})	g_x	g_y	g_z	Wavefunction
0.00	1.23	2.42	6.26	80.7%|±7/2⟩ + 9.0%|±1/2⟩ + 5.5%|±3/2⟩ + 4.8%|±5/2⟩
284.742	0.31	1.53	6.30	49.8%|±1/2⟩ + 27.9%|±3/2⟩ + 12.1%|±5/2⟩ + 10.3%|±7/2⟩
415.444	1.77	2.59	4.34	56.9%|±5/2⟩ + 27.5%|±3/2⟩ + 9.4%|±1/2⟩ + 6.2%|±7/2⟩
707.518	0.27	0.35	7.62	39.2%|±3/2⟩ + 31.9%|±1/2⟩ + 26.2%|±5/2⟩ + 2.9%|±7/2⟩

Table S10. Single_Aniso computed energy of the KDs, g and wavefuctions composition for **2**.

Energy (cm^{-1})	g_x	g_y	g_z	Wavefunction
0.00	5.00	3.81	1.26	96.3%|±1/2⟩ + 2.2%|±7/2⟩ + 0.9%|±5/2⟩ + 0.6%|±3/2⟩
172.193	0.23	2.30	5.25	63.9%|±3/2⟩ + 28.5%|±5/2⟩ + 7.5%|±7/2⟩ + 0.1%|±1/2⟩
366.903	1.24	1.89	4.80	37.0%|±5/2⟩ + 33.6%|±3/2⟩ + 26.8%|±7/2⟩ + 2.6%|±1/2⟩
653.837	0.16	0.22	7.78	63.5%|±7/2⟩ + 23.6%|±5/2⟩ + 1.9%|±3/2⟩ + 1.1%|±1/2⟩

Table S11. Single_Aniso computed energy of the KDs, g and wavefuctions composition for **3**.

Energy (cm^{-1})	g_x	g_y	g_z	Wavefunction
0.00	5.17	3.89	1.14	97.8% |±1/2⟩ + 1.2% |±5/2⟩ + 0.6% |±3/2⟩ + 0.4%|±1/2⟩
288.037	2.83	2.66	1.48	87.1% |±3/2⟩ + 9.8% |±5/2⟩ + 2.6% |±7/2⟩ + 0.6%|±1/2⟩
441.316	2.09	2.21	5.65	60.6% |±5/2⟩ + 27.0% |±7/2⟩ + 11.3% |±3/2⟩ + 1.0%|±1/2⟩
770.538	2.60×10^{-3}	4.48×10^{-2}	7.92	70.0% |±7/2⟩ + 28.6% |±5/2⟩ + 1.0% |±3/2⟩ + 0.4%|±1/2⟩

Table S12. Fitted exchange coupling constant J_{exch}, the calculated dipole–dipole interaction J_{dip} and the total J_{total} value between Yb(III) ions in **1**-**3** (cm^{-1}).

Complexes	J_{exch}	J_{dip}	J_{total}
1	-0.7096	0.0524	-0.6572
2	-0.3435	0.0376	-0.3059
3	-0.0906	0.0426	-0.0480

References

1. (a) G. Sheldrick, *Acta Crystallogr., Sect. A*, 2008, **64**, 112-122; (b) G. Sheldrick, *Acta Crystallogr., Sect. C*, 2015, **71**, 3-8.
2. O. V. Dolomanov, L. J. Bourhis, R. J. Gildea, J. A. K. Howard and H. Puschmann, *J. Appl. Cryst.*, 2009, **42**, 339-341.
3. M. Wedler, M. Noltemeyer, U. Pieper, H.-G. Schmidt, D. Stalke and F. T. Edelmarin, *Angew. Chem. Int. Ed.*, 1990, **29**, 894-896.
4. G. Li Manni, I. Fdez. Galván, A. Alavi, F. Aleotti, F. Aquilante, J. Autschbach, D. Avagliano, A. Baiardi, J. J. Bao, S. Battaglia, L. Birnoschi, A. Blanco-González, S. I. Bokarev, R. Broer, R. Cacciari, P. B. Calio, R. K. Carlson, R. Carvalho Couto, L. Cerdán, L. F. Chibotaru, N. F. Chilton, J. R. Church, I. Conti, S. Coriani, J. Cuéllar-Zuquin, R. E. Daoud, N. Dattani, P. Decleva, C. de Graaf, M. G. Delcey, L. De Vico, W. Dobrautz, S. S. Dong, R. Feng, N. Ferré, M. Filatov, L. Gagliardi, M. Garavelli, L. González, Y. Guan, M. Guo, M. R. Hennefarth, M. R. Hermes, C. E. Hoyer, M. Huix-Rotllant, V. K. Jaiswal, A. Kaiser, D. S. Kaliakin, M. Khamesian, D. S. King, V. Kochetov, M. Krośnicki, A. A. Kumaar, E. D. Larsson, S. Lehtola, M.-B. Lepetit, H. Lischka, P. López Ríos, M. Lundberg, D. Ma, S. Mai, P. Marquetand, I. C. D. Merritt, F. Montorsi, M. Mörchen, A. Nenov, V. H. A. Nguyen, Y. Nishimoto, M. S. Oakley, M. Olivucci, M. Oppel, D. Padula, R. Pandharkar, Q. M. Phung, F. Plasser, G. Raggi, E. Rebolini, M. Reiher, I. Rivalta, D. Roca-Sanjuán, T. Romig, A. A. Safari, A. Sánchez-Mansilla, A. M. Sand, I. Schapiro, T. R. Scott, J. Segarra-Martí, F. Segatta, D.-C. Sergentu, P. Sharma, R. Shepard, Y. Shu, J. K. Staab, T. P. Straatsma, L. K. Sørensen, B. N. C. Tenorio, D. G. Truhlar, L. Ungur, M. Vacher, V. Veryazov, T. A. Voß, O. Weser, D. Wu, X. Yang, D. Yarkony, C. Zhou, J. P. Zobel and R. Lindh, *J. Chem. Theory Comput.*, 2023, **19**, 6933-6991.
5. B. A. Heß, C. M. Marian, U. Wahlgren and O. Gropen, *Chemical Physics Letters*, 1996, **251**, 365-371.
6. P. Å. Malmqvist, B. O. Roos and B. Schimmelpfennig, *Chemical Physics Letters*, 2002, **357**, 230-240.
7. L. Ungur and L. F. Chibotaru, *Chem. Eur. J.*, 2017, **23**, 3708-3718.
8. (a) L. F. Chibotaru, L. Ungur and A. Soncini, *Angew. Chem. Int. Ed.*, 2008, **47**, 4126-4129; (b) L. Ungur, W. Van den Heuvel and L. F. Chibotaru, *New J. Chem.*, 2009, **33**, 1224-1230; (c) L. F. Chibotaru, L. Ungur, C. Aronica, H. Elmoll, G. Pilet and D. Luneau, *J. Am. Chem. Soc.*, 2008, **130**, 12445-12455.